Google4Habitat – a novel method for remote sensing-based habitat classification using Google Earth Engine

Gregory Egger, Stephan Preinstorfer, Marlene Kollmann, Isabell Becker, Emma Izquierdo-Verdiguier, Miriam Paul

ABSTRACT

Global and accelerating loss of biodiversity requires stronger management and protection of ecological resources. In Europe, various habitat types frequently need to be monitored within the framework of the Natura 2000 program. To achieve this, a robust monitoring tool, generating precise habitat maps, is crucial. Because of the specific conditions in mountainous areas, such as steep slopes and hard-to-reach areas that impede large-scale field surveys, remote sensing approaches are increasingly used to generate reliable maps. The novel classification method Google4Habitat, developed in this study, combines globally available satellite data (Sentinel/Landsat) with a series of site characteristics and upstream expert rules. Within Google Earth Engine, habitats are classified via spatial and temporal analysis based on spectral profiles and combined with factors such as elevation, vegetation height, surface roughness (based on LiDAR (light detection and ranging) data), geology, and indices for vegetation greenness (NDVI, normalized difference vegetation index), snow cover (NDSI, normalized difference snow index), and water (NDWI, normalized difference water index) in a supervised classification approach. The following questions were addressed: 1) Do the results meet the stringent habitat classification guidelines of the Red List and the requirements of Natura 2000? 2) What impact do the different qualities of input data have on the accuracy of the results? 3) Is this method suitable for capturing long-term changes in habitat distribution? We tested our model in Seebachtal, an alpine region that includes all habitat types from the montane to the nival zone and is one of the most untouched valleys in the Hohe Tauern National Park. The results are promising both in terms of habitat classification and delineation, largely meeting with the Natura 2000 guidelines. Due to their lower spatial resolution, Landsat data cannot fully detect small-area habitat types such as fens and still water. However, a comparison with the higher-resolution Sentinel-2 data shows that, in consideration of the entire study area, the classification accuracy using Sentinel-2 data did not significantly improve. Changes in habitat distribution over a 30-year-period were captured reliably. Overall, our model allows the rapid classification of large areas with high accuracy, opening new avenues for practical environmental management.

KEYWORDS

- Hohe Tauern National Park
- Sentinel
- Landsat
- alpine vegetation
- Natura 2000

Google4Habitat – eine neuartige Methode zur fernerkundungsbasierten Habitatklassifizierung in Google Earth Engine

ZUSAMMENFASSUNG

Der globale und sich beschleunigende Verlust der biologischen Vielfalt erfordert ein verstärktes Management und einen erhöhten Schutz der ökologischen Ressourcen. In Europa werden die verschiedenen Habitattypen im Rahmen von Natura 2000 regelmäßig erhoben. Dies erfordert ein zuverlässiges Monitoring-Tool, durch das sich die Habitattypen präzise erfassen und abgrenzen lassen. Aufgrund der herausfordernden Bedingungen in Gebirgslandschaften, die groß angelegte Geländeuntersuchungen erschweren, werden zunehmend Fernerkundungsansätze zur Erstellung zuverlässiger Habitatkarten eingesetzt. Das in dieser Studie entwickelte Klassifizierungsverfahren Google4Habitat kombiniert global verfügbare Satellitendaten (Sentinel/Landsat) mit einer Reihe von Standortparametern und vorgeschalteten Expertenregeln zur Ausweisung der Habitate. Dafür wurde in Google Earth Engine für jedes Habitat eine räumliche und zeitliche Analyse des Spektralprofils durchgeführt. Weiters wurden die Parameter Seehöhe, Vegetationshöhe, Oberflächenrauheit (basierend auf LiDAR-Daten (Light Detection and Ranging)), Geologie sowie Indizes bezüglich Vegetation (NDVI, normalisierter Differenzvegetationsindex), Schneedecke (NDSI, normalisierter Differenzschneeindex) und Wasser (NDWI, normalisierter Differenzwasserindex) ausgewertet, um mittels einer überwachten Klassifizierung die Habitate auszuweisen. Folgende Fragen wurden beantwortet: 1) Entsprechen die Ergebnisse den Habitatklassifizierungsrichtlinien der Roten Liste und den Anforderungen von Natura 2000? 2) Welchen Einfluss haben die unterschiedlichen Qualitäten der Eingabedaten auf die Genauigkeit der Ergebnisse? 3) Ist diese Methode geeignet, langfristige Veränderungen in der Habitatverteilung zu erfassen? Wir haben unser Modell im Seebachtal getestet, einer alpinen Region, die Habitattypen von der montanen bis zur nivalen Zone umfasst und zu den unberührtesten Tälern im Nationalpark Hohe Tauern zählt. Die Ergebnisse sind sowohl hinsichtlich der Habitatklassifizierung als auch der Abgrenzung vielversprechend und entsprechen weitgehend den Vorgaben der Roten Liste Kärnten und der Natura 2000 Richtlinien. Landsat-Daten können aufgrund der geringeren räumlichen Auflösung keine kleinräumigen Habitattypen

wie Moore und Stillgewässer vollständig erfassen. Ein Vergleich mit den räumlich höher aufgelösten Sentinel-2 Daten zeigt allerdings, dass über das gesamte Untersuchungsgebiet betrachtet, die Genauigkeit der Klassifizierung mittels Sentinel-2 Daten nicht wesentlich verbessert werden konnte. Die Veränderungen in der Habitatverteilung über einen Zeitraum von 30 Jahren wurden jedoch zuverlässig erfasst. Insgesamt ermöglicht unser Modell die rasche Klassifizierung großer Gebiete mit hoher Genauigkeit und eröffnet so neue Wege im Umweltmanagement.

INTRODUCTION

Against the background of the current biodiversity crisis and widespread habitat loss, the management, protection, and conservation of ecological resources have become significant global issues [1], [2]. In the EU, the Natura 2000 program has the objective of creating a network of ecologically valuable conservation areas in all member states. These conservation areas are often established with the aim of maximizing nature protection while minimizing conflicts with human activities [3]. The Natura 2000 network is set up in the framework of two different, but integrated, European directives: 79/409/EEC—Birds Directive and 92/43/EEC—Flora Fauna Habitat (FFH) Directive. As one of the most important instruments, the FFH Directive was established by the European Union in 1992. It requires states to constantly monitor the quality and sustainability of their Natura 2000 sites based on uniform and comprehensible criteria across the European Union. This frequently requires the mapping and monitoring of different vegetation classes and habitat types [4]. The resulting maps must fulfill stringent requirements in terms of habitat classification and delineation. For comparison, the requirements are 1:5,000 for the Red List Carinthia and 1:10,000 for the FFH Directive guidelines. However, given the diversity and dynamics of natural habitats, as a result of anthropogenic activities and natural disturbances, along with the low quantity of available reference plots, their precise classification is challenging [5]. For adequate habitat classification, the data need to be spatially explicit, available at fine scale to show local effects, and with a high temporal resolution [6], [7]. Although such data can be obtained via field sampling, the fieldwork required for the complete monitoring of such sites is labor-consuming and costly. In addition, the monitoring of vast areas requires numerous field workers, with a risk of the introduction of inter-operator errors [8].

In mountainous areas, vegetation is mainly influenced by habitat factors such as elevation, exposure, soil depth, moisture level, nutrient level, wind, seasonal variation, and duration of snow cover [9], [10], [11], [12], [13], [14]. Because of the specific plant sociological conditions, the production of reliable maps using remotely sensed images is not an easy task, and additional fieldwork is generally required. The common mapping approach produces habitat maps with low spatial resolution and diffuse habitat demarcation. This is because the potentially high heterogeneity of vegetation types is not captured through interpretation of information obtained via fieldwork and orthophotos. In this context, developing a robust monitoring system to generate precise and spatially inclusive maps is crucial to make informed decisions about habitat management and protection.

Recent decades have seen an unprecedented trend toward the use of remote sensing (RS) and geographic information systems (GIS) for habitat mapping and conservation-related issues [15], [16], [17], [18], [19], [20] at global, regional, and local scales [21], [22], and the availability of free data and software is constantly increasing [23], [24]. Using high-resolution satellite images, changes in surface properties can be mapped and linked with multiple indicators of changes in land conditions. In this context, RS enables rapid map production, especially for hard-to-reach regions [25]. Several authors have applied

RS satellite data for land use/land cover (LU/LC) classification, facilitating landscape observation, habitat mapping, assessment, and monitoring [5], [26], [27], [28], [29], [30], [31], [32], [33], [34], [35]. The use of satellite images versus orthophotos comes with several advantages: First, due to the use of a large number of spectral channels, more information can be extracted, albeit at a low spatial resolution. Second, the repetition rate is generally high because of the high temporal resolution.

Recently, there has been a trend to use open-access satellite archives such as those generated from MODIS (moderate-resolution image spectroradiometer), Landsat, and Sentinel in the RS of terrestrial ecosystems [36]. For example, MODIS data, with a 500-m resolution, have been applied to estimate different vegetation characteristics, such as leaf area index, biomass, and productivity [37], [38]. However, in many cases, a finer spatial resolution than that provided by MODIS is required [39], [40]. High spatial resolution of less than 10 m [41] largely increases the precision of the identification and characterization of small objects at spatial scales which were previously only available from airborne platforms.

To meet the stringent FFH Directive quality criteria, in particular, to obtain precise habitat demarcation, Sentinel data alone are not sufficient as they generate relatively coarse maps with a 10-m spatial resolution. For high-quality habitat classification, it is crucial to determine reference points, which requires expert knowledge in vegetation ecology. Such reference points need to be established in the field and can be supplemented with orthophotos. This allows for a supervised classification, combining a high classification level with expert knowledge.

Google Earth Engine (GEE) is a cloud-based computing platform that uses Google Cloud infrastructure to facilitate access to geospatial data and processing [42]. This platform gathers information from Landsat, Sentinel, and MODIS satellites, as well as data on climate models, temperature, and geophysical characteristics, managing large datasets [42], [43]. In geoscience and RS, GEE has become a powerful tool for RS applications and has been applied in fields such as vegetation and grassland monitoring [33], [34], [35], [44], mangrove mapping [45], LU/LC analysis [46], [47], [48], surface temperature [49], water area monitoring [50], [51], [52], [53], built-up area detection [54], [55], and mining impacts [56], among others.

Since 2008, when the Landsat image archive was opened [57], time series analysis of Landsat imagery has been thriving, with the rapid development of new algorithms and capabilities for change detection. The Landsat series has been collecting imagery of the Earth's surface since 1972, with a spatial resolution of 30 m, offering the longest possible time series and allowing comparisons with historical data [58]. In contrast, Sentinel-2 images, which became available in 2015, have a higher spatial resolution of 10 m and allow improved spatial resolution classification. Because of their high temporal resolution (Sentinel-2 has a 5-day revisit time instead of the 16-day interval provided by Landsat), they better enable the monitoring of vegetation and LU changes [59], [60] and can capture the effects of single disturbance events such as mudflows or avalanches. Although Sentinel-2 data allow a more detailed classification than Landsat data, they are not exceptionally suitable for habitat demarcation as they produce rather coarse maps. Further, for long-term comparisons, Landsat data, albeit with a lower resolution, need to be consulted. As commonly used data, light detection and ranging (LiDAR) data can be a valuable tool in habitat classification and provide important information. As our model can also be applied to past situations, for which LiDAR data are generally not available, we included LiDAR data to test the additional information value and to determine whether there is a loss of information without the use of LiDAR.

As a key parameter for investigating vegetation coverage, the NDVI (normalized difference vegetation index) can provide information on factors such as vegetation greenness and growth status, allowing the monitoring of seasonal, inter-annual, and long-term variations in vegetation structural, phenological, and biophysical parameters [61]. It is the most widely used vegetation index in RS applications [62], [63] and based on a simple band calculation, thereby enabling fast computation. This index exploits the fact that green healthy vegetation shows contrasting behavior in how it reflects red and near-infrared (NIR) radiation, differentiates habitat types based on biomass and is calculated as follows:

NDVI = (NIR – RED) / (NIR + RED),
where NDVI is the normalized difference vegetation index, NIR is the near-infrared band, and RED is the red band.

For Sentinel-2, the equation is NDVI = (B8 – B4) / (B8 + B4),
where NDVI is the normalized difference vegetation index, B8 is Band NIR (835.1 nm), and B4 is Band Red (664.5 nm).

For Landsat-8, the equation is NDVI = (SR_B5 – SR_B4) / (SR_B5 + SR_B4),
where NDVI is the normalized difference vegetation index, SR_B5 is Band 5 (near infrared) surface reflectance, and SR_B4 is Band 4 (red) surface reflectance.

In this study, we also employed the NDSI (normalized difference snow index) and NDWI (normalized difference water index).
Here, we propose the novel classification method Google4Habitat, version 1.0, using GEE, which allows the monitoring of various habitat types using RS data. To this end, Seebachtal in Hohe Tauern National Park was used as an experimental site (Figure 1). This area is part of the Natura 2000 network. Except for some areas in the outer valley, which are used for hay production and livestock grazing, most of the land has not been used since the end of the 19th century. We selected Seebachtal because it includes all habitat types from the montane to the nival zone and is one of the most untouched valleys in the Hohe Tauern. In addition, in 1994, area-wide vegetation maps were generated for this region, based on field observations [64]. However, because of the specific plant sociological conditions and the conditions in the field, the resulting maps are relatively coarse and therefore not suitable for use in our model.

Fig. 1

Figure 1: Impression of the upper Seebachtal valley, which is closed by the 3,361-m-high Hochalmspitze (center). This is followed by the Winklkees and extensive glacier forelands in the Lassacher Winkl. In the front are alpine grasslands. Source: Gregory Egger

Abbildung 1: *Foto des oberen Seebachtals, welches von der 3,361 m hohen Hochalmspitze (Bildmitte) abgeschlossen wird. Daran schließt sich das Winklkees mit ausgedehnten Gletschervorfelder im Lassacher Winkl an. Im Vordergrund befinden sich alpine Magerrasen. Quelle: Gregory Egger*

The aim of this study is to develop a method with high classification and delineation accuracy that allows a monitored classification and can be conferred to different habitat types, which is also important against the background of the monitoring of Natura 2000 sites. The global use of this method, across various climatic regions and habitat types, necessitates globally available site data (Landsat, Sentinel). In the supervised classification approach, the model is calibrated and trained using reference points of user-defined habitat types to generate the algorithm. Based on the reference points, the relation between specific geospatial conditions and the type of habitat is captured, allowing the prediction of the habitat types and the probability at which they occur. In contrast, in non-supervised classification approaches, statistically defined classes are automatically distinguished. Since the focus was on defined habitat types of the FFH Directive and Red List Carinthia, we used the supervised classification approach. The results are validated employing a subset of reference points alongside statistical metrics. The use of RS data allows the prediction of biotype maps and posterior monitoring of the area. The benefits of this novel approach are evident: large areas can be classified accurately and rapidly, with high efficiency, along with areas that are difficult to access. Various habitat types can be classified with high accuracy, close to that of terrain mapping and with precise delineation. Such an approach is important especially in the context of the Natura 2000 framework as it meets the stringent requirements in terms of habitat classification and delineation. This further opens new avenues for practical environmental protection.

Considering the different data availabilities and limitations, we address the following research questions:

- Do the habitat type demarcation and classification meet the stringent habitat classification guidelines of the Red List Carinthia and the requirements of Natura 2000?
- What impact do different sensor/satellite data have on the accuracy of the results?
- Is this novel method suitable to capture long-term changes in habitat types?

METHODS

Study area

Our study area was located in Seebachtal, which is part of the Hohe Tauern National Park in the state of Carinthia, Austria (Figure 2; E 13.1521745676888440, N 46.9899650250165877 to E 13.3234604899355809, N 47.0493634912617793). Seebachtal covers an area of approximately 52 km^2 and is situated at an elevation from 1,200 to 3,361 m. The climate is continental, with an average annual temperature of 5.2°C at 1,186 m and -5.8°C at 3,106 m. The average annual precipitation is 1,055 and 2,670 mm at 1,186 and 3,106 m, respectively. The area experiences 156 and 318 frost days at 1,186 and 3,106 m, respectively, with 110 and 353 days of snow cover (www.klimaatlas.ktn.gv.at). The vegetation is described in detail in the RESULTS section. Geomorphologically, Seebachtal is a glacially formed trough valley with rock basins deepened by Ice Age glaciers. The rubble-filled, flat trough floor suddenly merges into the steep, partly vertical trough walls. These end with a flatter trough shoulder, above which there are extensive cirques in the front section of the valley and steep, funnel-like valleys in the rear section. The higher valley areas are partly glaciated and merge into the rock faces of the summit and ridge regions. Geologically, Seebachtal is located in the Hohe Tauern Window and characterized by the central gneisses and rocks of the surrounding schist shell [65].

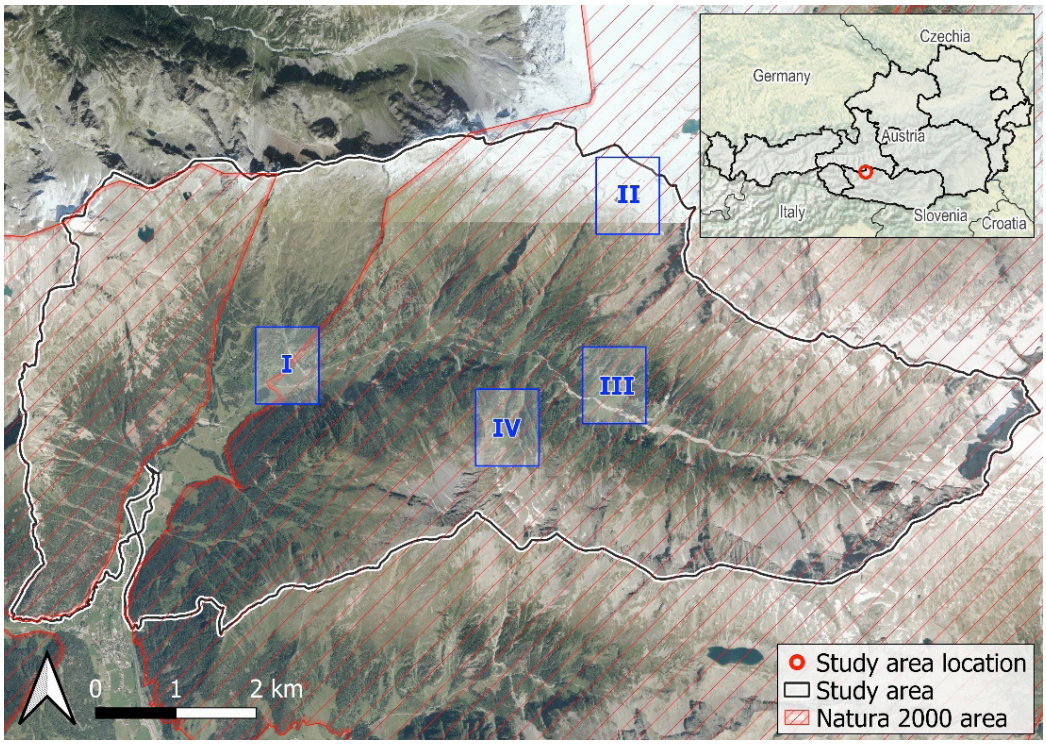

Fig. 2

Figure 2: Overview of the study area in Seebachtal, Hohe Tauern National Park, showing the Natura 2000 area (shaded in red). Reference zones: I: Valley entrance, II: High-altitude mountain, III: Rear valley floor, IV: Transition from forest – shrub – dwarf shrub – nutrient-poor grassland – rock debris on the southern slope. Source: Own figure (orthophoto derived from basemap.at)

Abbildung 2: *Übersicht über das Untersuchungsgebiet im Seebachtal, Hohe Tauern Nationalpark, mit den Natura 2000 Flächen (rot schraffiert). Referenzgebiete: I: Taleingang, II: Hochgebirge, III: hinterer Talboden, IV: Übergang Wald – Gebüsch – Zwergstrauchheiden – Magerrasen – Schutt am Südhang. Quelle: Eigene Abbildung (Orthofoto basierend auf basemap.at)*

Classification scheme

Based on area-wide mapping in 1992, Seebachtal contains approximately 60 different vegetation subtypes [64]. For simplicity, in this study, we classified the 10 most dominant vegetation types, namely grey alder forest, spruce forest, larch/Swiss pine forest, green alder shrub, mountain pine shrub, dwarf shrub, tall forb community, nutrient-poor grassland, nutrient-rich grassland, and fen, along with rock, glacier/snow field, rock debris, and still water, totaling 14 habitat types across the study region.

Habitat classification and segmentation

Habitat classification was performed in GEE using JavaScript, and the geospatial data were in the form of raster files (GeoTIF) and vector files (ESRI Shapefile). GEE provides satellite images which were filtered for cloud-free images of our study area in the specific time range. As each pixel contains information on cloud cover, this information was used to create a cloud mask, which removed all cloudy pixels left within the images. All images with more than 30% cloud coverage were excluded. The total number of used Sentinel-2 images with a cloud cover below 30% was 49, and the number of available images of Landsat with a cloud cover lower than 30% was 22. However, for some months, we did not have any available images due to clouds, as was the case in March, April, and May. Therefore, the NDVI was not calculated monthly as for Sentinel-2 but quarterly. Consequently, some pixels had to be filled in using values from the same quarter of the previous year or, in the case of remaining gaps, with the median of the surrounding area. In this sense, GEE allowed the geospatial and statistical analysis of individual bands of raster images. The multi-step process is shown in Figure 3 and described in detail in the following section.

First, we selected from 54 to 375 reference points (mean: 143) per habitat type (preferably distributed in the entire study area) for model calibration and validation and performed expert-based classification of the habitat type based on orthophotos (as of 2022 or 1992;

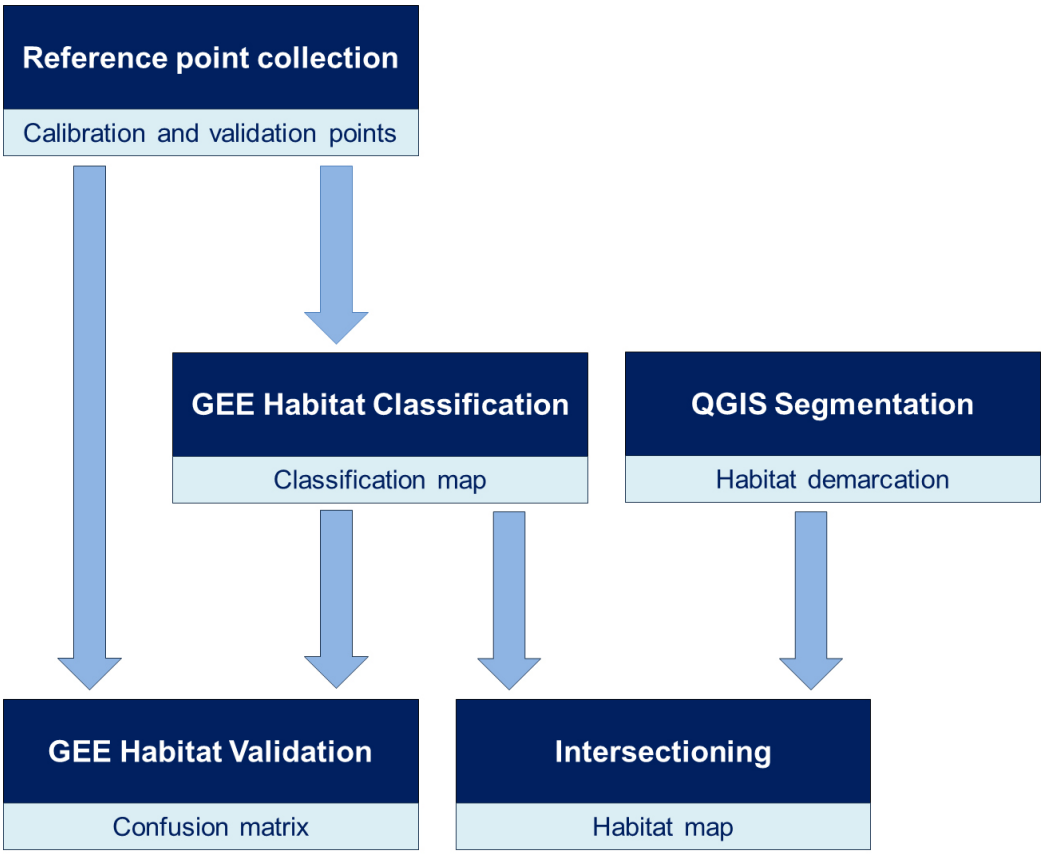

Fig. 3

Figure 3: Flow diagram showing the workflow for habitat classification and segmentation in Google4Habitat. Source: own figure

Abbildung 3: *Flussdiagramm mit der Vorgehensweise der Klassifizierung und Segmentierung von Habitaten in Google4Habitat. Quelle: eigene Abbildung*

basemap.at). The NDVI values were calculated from red and NIR bands of the images with a cloud cover of less than 30% (Sentinel-2), masking the pixels classified as cloud cover in the scene classification map. The same process was followed to calculate the monthly NDWI values only for the snow-free months (for Sentinel-2 and Landsat-8: from July to August; for Landsat-5: from April to September), using NIR and short-wavelength infrared bands. Additionally, LiDAR data (elevation model [DEM] and surface model [DSM]) were downloaded from https://kagis.ktn.gv.at/Geodaten/H%c3%b6hendaten%20-%20 Download. Slope was calculated from the DEM using the "slope" tool in QGIS. Surface roughness was calculated from the DSM using the "roughness" tool in QGIS. Vegetation height was calculated by subtracting the elevation model from the surface model (DSM – DEM), and the resulting values were reclassified into three height classes (< 1 m, 1–7 m, > 7 m). The data were stacked, and the values of the reference points were extracted. Two-third of the reference points were allocated for training a random forest (RF) classifier using default parameters, and the remaining one-third was kept for validating the model. The use of the RF classifier was based on its good characteristics and performance regarding complex decision boundaries [66], [67]. To measure the quality of the RF classifier, Cohen's kappa (κ) and the confusion matrix (CM) were determined. For the maps generated without LiDAR data, a globally available elevation model was used instead (NASA/USGS/JPL-Caltech). Finally, we created a mask for snow-covered surfaces by calculating the NDSI (normalized difference of green and short-wave infrared) in August. This mask was blended with the RF classification results to improve snow detection.

The procedure used for Landsat imagery was similar to that used for Sentinel-2, as described above. The main difference was the temporal resolution of the NDVI calculation. Whilst the NDVI values were calculated monthly for Sentinel-2 data, for Landsat, we calculated quarterly NDVI values. Due to the smaller number of available images, some

pixels lacked usable values and were masked. These pixels were filled in using values from the same quarter of the previous year or, in the case of remaining gaps, with the median of the surrounding area. To determine the additional information of LiDAR data, Map 2a was generated with Sentinel-2 data only and compared with Map 1a1 (generated with Sentinel-2 and LiDAR data). Table 1 provides an overview of the input data sources used for habitat classification and the resulting maps.

Tab. 1

Input data source	Map 1a1	Map 1a2	Map 2a	Map 3a	Map 5a
Reference points 2022 (aerial photo, basemap.at)	x		x	x	
Reference points 2022 & corrected reference points 2022		x			
Reference points 2002					x
LiDAR: DEM, slope inclination & direction, surface roughness, vegetation height classes (1 m, 1–7 m, > 7 m); (https://kagis.ktn.gv.at, CC-BY-4.0)	x	x		x	
DGM and slope (NASA/USGS/JPL-Caltech)			x		x
Sentinel-2, 2022 (Copernicus Sentinel data 2022)	x	x	x		
Landsat-8, 2022 (Landsat-8 images courtesy of the U.S. Geological Survey)				x	
Landsat-5, 1992 (Landsat-5 images courtesy of the U.S. Geological Survey)					x
Scaling and offset				x	x
NDVI, monthly	x	x	x		
NDVI, quarterly/per season				x	x
NDWI, July to August	x	x	x		
NDWI, April to September				x	x
NDSI (Copernicus Sentinel data 2022), August	x	x	x		

Table 1: Input data and data sources used for habitat classification using Google Earth Engine and the resulting maps.
LiDAR = light detection and ranging;
DEM = digital elevation model;
NDVI = normalized difference vegetation index;
NDWI = normalized difference water index;
NDSI = normalized difference snow index

Tabelle 1: *Eingabedaten und Datenquellen für die Habitatklassifizierung mit Google Earth Engine und die Ergebniskarten. LiDAR = Licht- und Entfernungsmessung; DEM = Digitales Geländemodell; NDVI = normalisierter differenzierter Vegetationsindex; NDWI = normalisierter differenzierter Wasserindex; NDSI = normalisierter differenzierter Schneeindex*

To obtain habitat maps with precise delineation, segmentation was performed in QGIS [68], using a series of sub-steps. First, we automatically delineated (i.segment, QGIS) the different habitat structures on an orthophoto (Land Kärnten - KAGIS - https://kagis.ktn.gv.at, CC-BY-4.0). Second, the delineation map was intersected with the classification map, and the dominant habitat types in each sub-segment were transferred from the classification raster to the delineation vector file (using Zonal Statistics). In a third step, we combined the neighboring sub-segments of the same habitat type (Dissolve) into segments, and fourth, we smoothed the resulting polygons (v.generalize, QGIS).

Generated maps

The maps generated using different input sources and reference points are shown in Table 2.

Tab. 2

Map	Map type	Input source	Reference points (year)
1a1	Classification map	Sentinel + LiDAR	2022
1a2 (Suppl. Figure 1)	Classification map	Sentinel + LiDAR	Corrected for 2022
1b (Suppl. Figure 2)	Segmentation map of Map 1a1	Sentinel + LiDAR	2022
2a (Suppl. Figure 3)	Classification map	Sentinel	2022
2b (Suppl. Figure 4)	Segmentation map of Map 2a	Sentinel	2022
3a (Suppl. Figure 5)	Classification map	Landsat + LiDAR	2022
3b (Suppl. Figure 6)	Segmentation map of Map 3a	Landsat + LiDAR	2022
4 (Suppl. Figure 7)	Classification map	Landsat	2022
5a (Suppl. Figure 8)	Classification map	Landsat	2002, trained on orthophotos from 1992 and Landsat data from 2002

Table 2: Overview of the generated maps and input sources

Tabelle 2: *Übersicht über die erstellten Karten und Datenquellen*

Capturing long-term habitat changes

To detect long-term changes in habitat types, we generated Map5a, which was trained on Landsat-5 images from 1992 and supplemented with reference points for 2022. This allowed us to determine habitat changes within a 30-year period.

RESULTS

Habitat type distribution using Google4Habitat

The use of various combinations and approaches (such as Sentinel/Landsat data, with/without LiDAR, with/without correction points) resulted in different maps. Table 3 shows the proportions of the different habitat types in relation to the entire area in the respective maps. The mean kappa value is 0.69, ranging from 0.66 to 0.76. The average producer's accuracy, indicating how well the reference pixels are classified, is 71%, with a range from 12% to 100% (Table 4, additional maps are provided in the Supplementary Material).

Tab. 3

Habitat type (%)/Map	1a1	1a2	1b	2a	3a	4	5a
Grey alder forest	2.3	1.2	2.3	2.8	1.9	3.2	2.8
Spruce forest	15.2	14.6	15.6	15.6	16.3	16.2	19.1
Larch/Swiss pine forest	8.7	9.2	9.2	9.2	9.4	9.1	8.9
Green alder shrub	2.3	2.1	1.8	1.3	2.8	2.1	1.4
Mountain pine shrub	3.4	3.3	3.3	3.3	2.6	2.9	3.7
Dwarf shrub	3.2	3.1	3.1	3.3	3.4	3.0	4.4
Tall forb community	1.7	1.9	1.7	1.7	1.6	1.6	1.4
Nutrient-poor grassland	21.0	20.9	21.2	21.6	20.0	21.5	20.2
Nutrient-rich grassland	2.5	4.3	2.4	1.8	2.2	1.6	1.4
Fen	0.3	0.3	0.3	0.2	0.2	0.1	0.2
Rock	16.0	16.9	15.5	15.8	15.7	14.7	14.2
Glacier/snow field	2.3	1.8	2.3	2.1	2.2	2.1	2.8
Rock debris	20.9	20.3	21.1	21.1	21.5	21.4	19.0
Still water	0.1	0.2	0.1	0.1	0.2	0.6	0.4
∑	*100*	*100*	*100*	*100*	*100*	*100*	*100*
kappa	*0.7*	*0.76*	*n.a.*	*0.75*	*0.70*	*0.66*	*0.66*

Table 3: Habitat type distribution (%) in Seebachtal based on the different maps. For map information, see Table 2 (n.a.: not applicable)

Tabelle 3: *Habitattypenverteilung (in %) im Seebachtal anhand der verschiedenen Karten. Für Informationen zu den einzelnen Karten, siehe Tabelle 2 (n.a.: nicht zutreffend)*

Tab. 4

Habitat type/Map	1a1	1a2	1b	2a	3a	4	5a
Grey alder forest	92	69	88	92	76	55	68
Spruce forest	93	89	88	92	91	79	86
Larch/Swiss pine forest	83	77	77	80	83	63	57
Green alder shrub	52	63	89	30	56	24	22
Mountain pine shrub	90	77	79	90	63	62	43
Dwarf shrub	53	53	66	53	63	51	38
Tall forb community	62	83	64	67	57	42	71
Nutrient-poor grassland	89	87	76	94	80	81	85
Nutrient-rich grassland	32	74	64	36	12	60	12
Fen	86	36	90	79	86	49	64
Rock	72	87	83	68	68	74	72
Glacier/snow field	74	58	67	68	35	49	39
Rock debris	84	80	75	81	80	81	71
Still water	89	100	100	89	89	62	94

Table 4: Producer's accuracy values (%) for the different habitat types in the respective maps. For map information, see Table 2

Tabelle 4: *Produzenten-Genauigkeit (%) für die verschiedenen Habitattypen in den jeweiligen Karten. Für Informationen zu den einzelnen Karten, siehe Tabelle 2*

Classification map showing the current situation (2022)

Map 1a1 was generated using Sentinel-2 data, LiDAR data, and reference points from 2022 and is the current classification map of Seebachtal in GEE (Figure 4). Map 1a1 is the most accurate one in terms of the different habitat types and shows the actual situation. The lower valley floor area and lower hillsides are dominated by nutrient-rich grassland and grey alder forests. In the subalpine part, spruce forest dominates (15%), transitioning into larch and Swiss pine forest in the upper parts. Generally, forest accounts for one quarter of the total region. On south to south-eastern slopes of the valley, adjacent to the forest, large areas of mountain pine shrub occur, whereas the northwestern and northern slopes are dominated by dwarf shrubs. Nutrient-poor grassland areas are found in the alpine zone and gradually transition into rock debris and rock.

The different forest types, mountain pine shrubs, nutrient-poor grassland, and fens had a very high producer's accuracy of approx. 80% to 95%. Grey alder forests, dwarf shrub areas, rocks, glaciers, and snow fields were classified with a moderate to high producer's accuracy from 50% to 75%. A low producer's accuracy was noted for nutrient-rich grassland (32%), which was frequently misclassified as nutrient-poor grassland and tall forb areas, in some cases also as fen and forest areas. The average producer's accuracy is 75%, ranging from 32% (intensive grassland) to 93% (spruce forest) (Table 5).

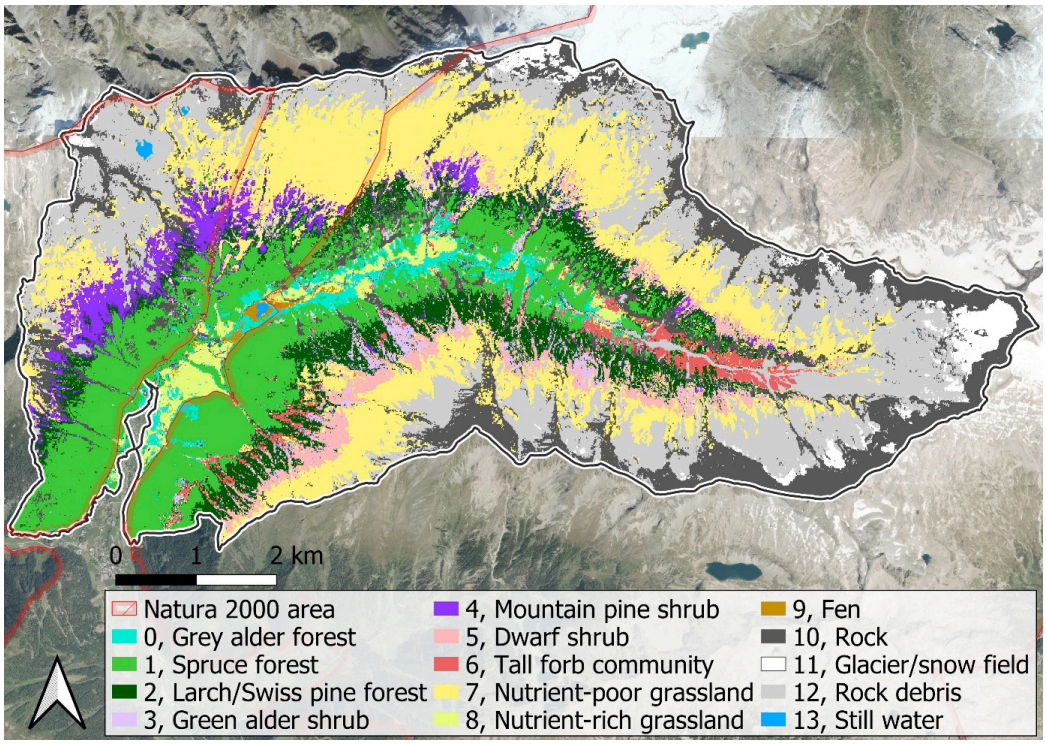

Fig. 4

Figure 4: Map 1a1, based on Sentinel-2 data, LiDAR data, and reference points for 2022.
Source: own figure

Abbildung 4: *Karte 1a1, erstellt mit Sentinel-2 Daten, LiDAR Daten und Referenzpunkten für 2022.*
Quelle: eigene Abbildung

Tab. 5

	RS model	Grey alder forest	Spruce forest	Larch/Swiss pine forest	Green alder shrub	Mountain pine shrub	Dwarf shrub	Tall forb community	Nutrient-poor grassland	Nutrient-rich grassland	Fen	Rock	Glacier/snow field	Rock debris	Still water	Total	*Producer's accuracy*
Field reference		**0**	**1**	**2**	**3**	**4**	**5**	**6**	**7**	**8**	**9**	**10**	**11**	**12**	**13**		
Grey alder forest	0	**92**	8	0	0	0	0	0	0	0	0	0	0	0	0	100	*0.92*
Spruce forest	1	0	**93**	4	0	1	0	0	0	0	0	2	0	0	0	100	*0.93*
Larch/Swiss pine forest	2	2	10	**83**	2	3	0	0	0	0	0	0	0	0	0	100	*0.83*
Green alder shrub	3	7	0	15	**52**	4	11	7	0	0	0	4	0	0	0	100	*0.52*
Mountain pine shrub	4	0	0	7	0	**90**	0	0	3	0	0	0	0	0	0	100	*0.90*
Dwarf shrub	5	0	0	0	0	3	**53**	0	45	0	0	0	0	0	0	100	*0.53*
Tall forb community	6	0	0	0	0	0	10	**62**	5	24	0	0	0	0	0	100	*0.62*
Nutrient-poor grassland	7	0	0	1	0	2	6	1	**89**	1	0	1	0	1	0	100	*0.89*
Nutrient-rich grassland	8	0	0	8	4	4	8	16	28	**32**	0	0	0	0	0	100	*0.32*
Fen	9	0	0	0	0	0	0	0	14	0	**86**	0	0	0	0	100	*0.86*
Rock	10	0	3	0	0	1	0	0	3	0	0	**72**	6	15	0	100	*0.72*
Glacier/snow field	11	0	0	0	0	0	0	0	0	0	0	10	**74**	16	0	100	*0.74*
Rock debris	12	0	0	0	0	0	0	0	3	0	0	7	7	**84**	0	100	*0.84*
Still water	13	6	0	0	0	0	0	0	0	0	6	0	0	0	**89**	100	*0.89*

Table 5: Confusion matrix for Map 1a1, including producer´s accuracy values

Tabelle 5: *Fehlermatrix für Karte 1a1 mit producer's accuracy Werten*

Corrected classification using additional reference points

Map 1a2 was generated using Sentinel-2 data, LiDAR data, and corrected reference points from 2022 (Supplementary Figure 1). Based on the overall kappa value, this map is most accurate; however, in terms of the different habitat types, Map 1a1 has a higher overall accuracy. The use of additional reference points for nutrient-rich grassland was necessary as in Map 1a1, this habitat type on the lower valley floor was frequently misclassified as grey alder forest. However, as shown in the confusion matrix, the overall accuracy was not significantly improved. Although with this approach, nutrient-rich grassland was classified with a higher accuracy, the accuracy for the other habitat types decreased. The average producer's accuracy is 74%, ranging from 36% (fen) to 100% (still water) (Supplementary Table 1).

Classification without LiDAR

Map 2a was generated using Sentinel-2 data and reference points for 2022, without additional information such as vegetation height and surface roughness via LiDAR data (Supplementary Figure 3). Habitat classification without the use of LiDAR data only had a slight impact on the classification accuracy. One exception is the green alder shrub area, for which the classification accuracy decreased from 0.52 (Map 1a1) to 0.3. The average producer's accuracy is 73%, ranging from 30% (green alder shrub) to 94% (nutrient-poor grassland) (Supplementary Table 2).

Classification using Landsat instead of Sentinel-2 data

Map 3a was generated using Landsat data, LiDAR data, and reference points for 2022 to determine the advantages of Sentinel over LiDAR data. Overall, the distribution of the habitat types is similar to that in Map 1a1, although the map has a lower spatial resolution and is therefore considerably coarser (Supplementary Figure 5). As shown in the confusion matrix, the average producer's accuracy is 67%, ranging from 12% (nutrient-

rich grassland) to 91% (spruce forest) (Supplementary Table 3). By intersecting Map 3a with Map 1a1, to compare the use of Landsat with that of Sentinel data, we obtained an average producer's accuracy of 59%, with a minimum of 24% (green alder shrub) and a maximum of 81% (nutrient-rich grassland and rock debris) (Supplementary Table 4).

Segmentation to obtain habitats with precise delineation

Map 1b is the segmentation map of Map 1a1, which shows the current situation of Seebachtal (Supplementary Figure 2). Based on the confusion matrix of the intersection of Maps 1b and 1a1 (Supplementary Table 5), forest areas could be classified with high producer's accuracy (80%–90%). Generally, all large-scale, homogeneous habitats were classified accurately (with a high to very high producer's accuracy). A moderate classification accuracy was obtained for small-area habitats with a patchy distribution throughout the study site, such as green alder shrub and fen areas, along with dwarf shrub and tall forb communities. The classification accuracy is particularly low for green alder shrub habitats. Generally, the segmentation results deviate around 10%–20% from the classification results, especially for areas that account for less than 200 m^2. This clearly shows that such standardization comes at the expense of small habitats. The average producer's accuracy is 80%, with a range from 58% (larch/Swiss pine forest) to 99% (still water) (Supplementary Table 5). Figures 5, 6, 7, and 8 illustrate the segmentation process to obtain precise habitat delineation for Reference Zones I–IV, respectively, of the study area (see Figure 2). In these figures, map a represents the classification map obtained using GEE based on Sentinel data, map b shows the delineation of different habitat structures on the orthophoto, and map c is the segmentation map, obtained by extracting the values of map a and adding them to the segments of map b. For this, the neighboring sub-segments of the same habitat type were merged.

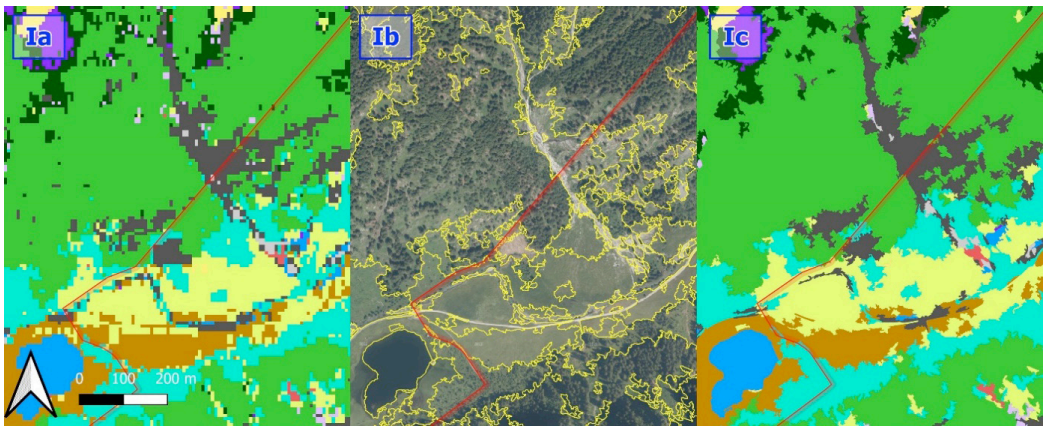

Fig. 5

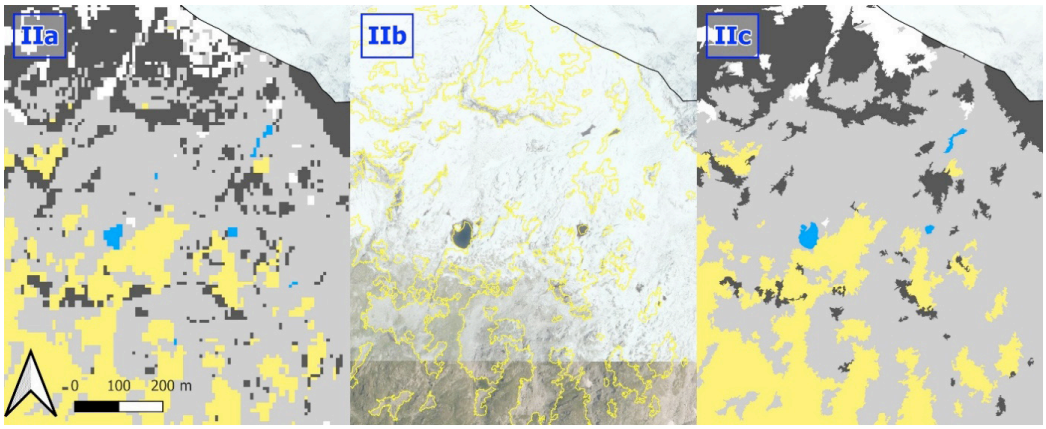

Fig. 6

Figure 5: Classification map (Ia), delineation map using the orthophoto (Ib), and segmentation map (Ic) for the valley entrance. For habitat types, see Figure 4, and for the location of Reference Zones, see Figure 2. Source: own figure

Abbildung 5: *Klassifizierungskarte (Ia), Abgrenzungskarte anhand des Orthofotos (Ib) und Segmentierungskarte (Ic) für den Taleingang. Habitattypen siehe Abbildung 4, und für die Lage der Referenzgebiete siehe Abbildung 2. Quelle: eigene Abbildung*

Figure 6: Classification map (IIa), delineation map using the orthophoto (IIb), and segmentation map (IIc) for the high-altitude mountain. For habitat types, see Figure 4, and for the location of Reference Zones, see Figure 2. Source: own figure

Abbildung 6: *Klassifizierungskarte (IIa), Abgrenzungskarte anhand des Orthofotos (IIb) und Segmentierungskarte (IIc) für das Hochgebirge. Habitattypen siehe Abbildung 4, und für die Lage der Referenzgebiete siehe Abbildung 2. Quelle: eigene Abbildung*

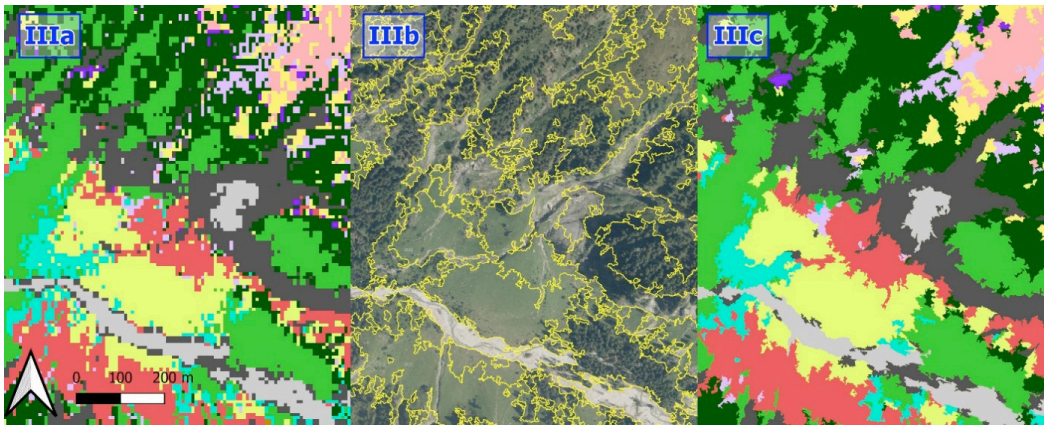

Fig. 7

Figure 7: Classification map (IIIa), delineation map using the orthophoto (IIIb), and segmentation map (IIIc) for the rear valley floor. For habitat types, see Figure 4, and for the location of Reference Zones, see Figure 2. Source: own figure

Abbildung 7: *Klassifizierungskarte (IIIa), Abgrenzungskarte anhand des Orthofotos (IIIb) und Segmentierungskarte (IIIc) für den hinteren Talboden. Habitattypen siehe Abbildung 4, und für die Lage der Referenzgebiete siehe Abbildung 2. Quelle: eigene Abbildung*

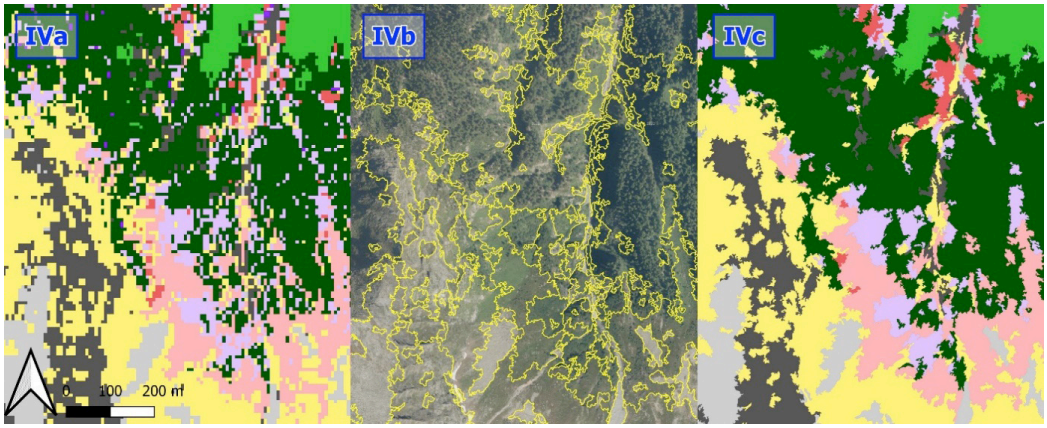

Fig. 8

Figure 8: Classification map (IVa), delineation map using the orthophoto (IVb), and segmentation map (IVc) for the transition zone from forest – shrub – dwarf shrub – nutrient-poor grassland – rock debris on the southern slope. For habitat types, see Figure 4 and for the location of the Reference Zones see Figure 2. Source: own figure

Abbildung 8: *Klassifizierungskarte (IVa), Abgrenzungskarte anhand des Orthofotos (IVb) und Segmentierungskarte (IVc) für den Übergang Wald – Gebüsch – Zwergstrauchheiden – Magerrasen – Schutt am Südhang. Habitattypen siehe Abbildung 4 und für die Lage der Referenzgebiete siehe Abbildung 2. Quelle: eigene Abbildung*

Capturing long-term changes in habitat types

Map 5a was generated using Landsat data only, supplemented with reference points for 2002 and trained on Landsat-5 imagery from 1992 (Supplementary Figure 8). Although for this map, there were no LiDAR data available, the difference to Map 3a, which was generated using Landsat and LiDAR data, is low. However, the forest area is markedly higher in Map 5a compared to the reference map because nutrient-rich grassland

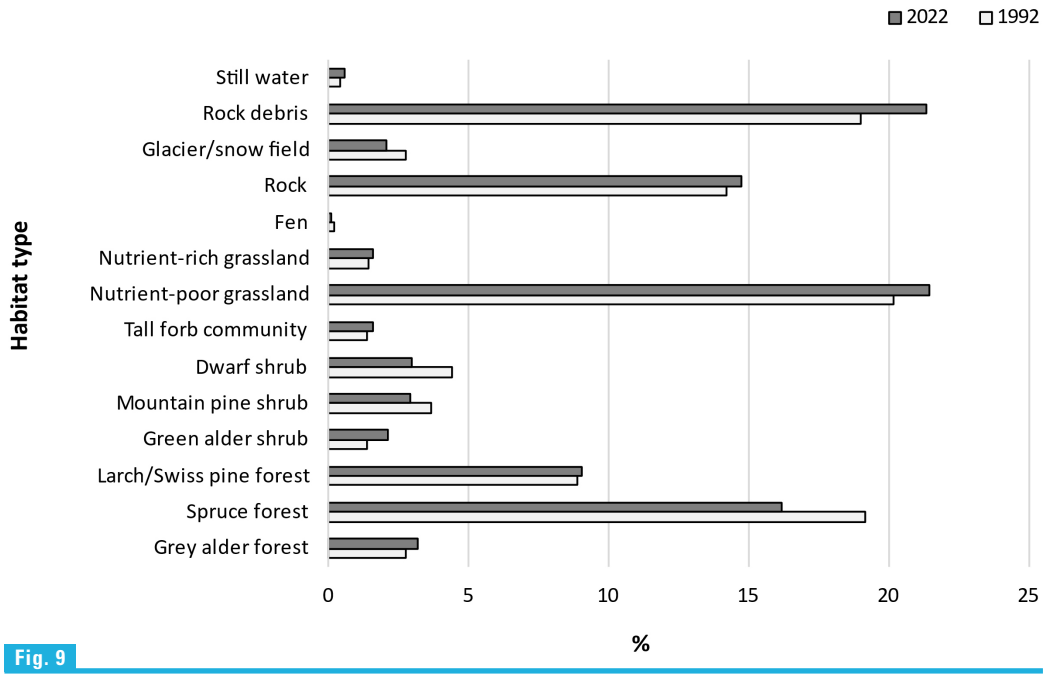

Fig. 9

Figure 9: Percentages of the different habitat types in 1992 and 2022. Source: own figure

Abbildung 9: *Prozentuale Anteile der verschiedenen Habitattypen in 1992 und 2022. Quelle: eigene Abbildung*

was frequently misclassified as grey alder forest. As shown in the confusion matrix, the average producer's is 59%, ranging from 12% (nutrient-rich grassland) to 94% (still water) (Supplementary Table 6). By intersecting Map 5a with Map 4, to capture long-term changes in habitat types, we obtained an average producer's accuracy of 69%, ranging from 36% (nutrient-rich grassland) to 89% (still water) (Supplementary Table 7). Figure 9 shows the differences in the percentages of the different habitat types between 1992 and 2022, indicating the long-term changes.

DISCUSSION

Can Google4Habitat meet the stringent habitat classification and delineation guidelines of the Red List Carinthia and the requirements of Natura 2000?

The physical environment is one of the most important factors impacting the spatial heterogeneity of the landscape in mountainous areas [69], [70]. In a complex system of site factors, topography creates a patchwork-like pattern of small-scale habitats within the ecological space, indirectly influencing alpine vegetation [71]. The vegetation distribution in alpine areas is mainly characterized by factors such as climate, soils, geology, and the frequency and intensity of disturbances [72]. For the mapping of these habitats, a GIS approach is most appropriate [73], and in the last decades, RS data have been widely applied in vegetation and habitat mapping [72].

The habitat types classified using our novel RS-based approach largely correspond to the habitat/group types designated in the Red List and Natura 2000 guidelines [74], [75], [76] Our model correctly classified areas with a minimum of 100 m^2 and obtained a precise delineation for habitats with a minimum size of 200 m^2. These values are considerably below the requirements of the Red List Carinthia and the FFH Directive guidelines. The map scale obtained with our model is 1:5,000 for classification and 1:500 for delineation. For comparison, the requirements are 1:5,000 for the Red List and 1:10,000 for the FFH Directive guidelines. Large-area habitats, such as grey alder and spruce forests, were frequently classified with high accuracy (above 90%). Similarly, using Sentinel data for the mapping of forest areas, other authors obtained overall accuracies of 94% in northern China [77], 32% in Lower Austria [78], and between 80% and 90% worldwide [79]. Although rock/rock debris could be classified with a moderate to good accuracy (72%/84%), it should be noted that, according to the FFH guidelines, these classes are only habitat types when they contain pioneer vegetation, requiring slight modifications when generating area-wide FFH maps. As the occurrence of rock debris is subject to seasonal changes, i.e., surface settlement by pioneer species, and successional changes, in the vegetation season, rock debris can be misclassified as, e.g., nutrient-poor grassland. Similarly, fens, which have a patchy distribution pattern and are subject to early vegetation succession [80], are difficult to classify accurately, and additional reference points from the field were necessary to obtain a satisfactory classification. Kopeć et al. [80], using the random forest classification method for alkaline fens in a Natura 2000 habitat in Poland, obtained a classification accuracy of 91%, slightly higher than the 86% obtained in our study [80]. Deviations from the actual conditions were mainly noted for ecologically similar habitat types that were distributed throughout the study site in a patchwork-type pattern. In mixed habitat types, the different habitats are difficult to classify using RS techniques, especially when they occupy only small areas (in our case, below 100 m^2), making accurate classification extremely difficult. However, these differences have a low relevance, depending on the scale of the produced map and the exact definition. It must be noted that, however, the nutrient-rich grassland areas at the valley floor were

frequently misclassified as green alder forest areas, with a low accuracy of 32%, leading to map errors. In relation to the overall number of pixels, the number of reference points is, however, extremely low, which means that the confusion matrix alone has a limited validity. Only after the use of additional reference points, the respective pixels and habitat types, including those in the surrounding areas, were classified correctly, and map errors could be corrected. However, this approach requires searching for errors using orthophotos, which is time- and labor-consuming. Another issue is the fact that with the use of new reference points in random forest, new calibration and validation points are established randomly, and the resulting algorithm has an impact on the classification of all habitat types. This results in slight deviations of habitat delineations which are, in our case, negligible. Overall, our findings largely agree with the classification outcomes reported for this area by Egger [64]. The accuracy results obtained here are promising, recommending the further use of Google4Habitat for Natura 2000 monitoring.

How do the different input data impact the accuracy of the results?

Both Maps 1a1 and 1a2 indicate the importance of the different input data. The combination of LiDAR data with multispectral imagery can result in considerably higher classification accuracies [81]. To determine the potential of LiDAR in habitat classification, we tested our model with and without the use of LiDAR data. When LiDAR height parameters (vegetation height and surface roughness) were included in the model, the overall classification accuracy was not significantly improved. Without the use of LIDAR data, grey alder and spruce forests were still classified with an accuracy of 92%, and for nutrient-poor grassland, a high accuracy of 94% was obtained. However, the classification accuracy for green alder shrub areas decreased from 52% to 30%, indicating a considerable error. Generally, although LiDAR data are important input data for the differentiation of vegetated areas, to further classify such areas as either open green, shrub, or forest areas, the use of upstream rules, based on expert knowledge, is crucial. As LiDAR provides the altitude information needed for discriminating among certain habitat classes, in the random forest classifier, general rules can be set. Areas with a vegetation height below 1 m can be classified as non-forest areas, a vegetation height of 1 to 7 m indicates shrub areas, and sites with a vegetation height above 7 m are classified as forests. Although this might lead to the misclassification of young forest sites as shrub sites or even open areas, as LiDAR is blind to the type of measured object, it still leads to a higher classification accuracy as forest areas are always classified correctly.

The classification accuracies of two different approaches, namely using Sentinel-2 and Landsat-8 data, were compared to determine the performance of different RS data. Sentinel-2 offers improved data compared to the low-spatial-resolution Landsat-8 data [82]. With a 10-m spatial resolution, Sentinel data facilitate the detailed exploration of different habitat types. The other valuable characteristics of Sentinel-2 data are the high temporal resolution of 5 days [59] and the availability of red-edge bands with multiple applications [83]. These features provide excellent opportunities for detailed habitat mapping at a fine scale. In contrast, Landsat-8 uses only 9 spectral bands (as opposed to 13 for Sentinel-2) and has a lower temporal resolution of 16 days [60]. Hence, the number of cloud-free images is considerably lower, impeding the generation of monthly data series, and only seasonal changes can be captured correctly.

Although in our study site, numerous habitat types showed a patchwork-like distribution, the use of Sentinel-2 data, with a higher spatial resolution, did not significantly improve the classification accuracy. This indicates that for most habitat types, the difference between pixel sizes of 10 x 10 m and 30 x 30 m is not decisive, and for areas of the size of our study

site, Landsat data are generally sufficient. Similarly, in a previous study on crop monitoring, the use of Sentinel-2 data resulted in only slightly higher accuracy values compared to the use of Landsat data (with a difference between 1% and 3%), depending on the classifier applied [84]. According to a recent review, due to the high spatial resolution, Sentinel-2 data can obtain higher accuracies compared to other medium-resolution satellite images [83]. However, in our study, for small-area habitat types, such as fens and still water, the use of Landsat data resulted in a considerable information loss because of the lower spatial resolution.

Can Google4Habitat capture long-term changes in habitat types?

Considering the entire study area, the difference in the habitat type net balance between 1992 and 2022 is low (1%–2%) and within the normal error rate. However, the net balance alone does not provide reliable information about long-term changes. In a further step, we therefore intersected Map 4 (1992) with Map 5a (2022) to capture potential progression/retrogression over a period of 30 years. As we only had data from two time points, we only provide snapshots of the habitat conditions for these two years, and the focus was on long-term changes and not on change patterns. The resulting succession map allows a direct comparison of all pixels and provides information regarding the change dynamics in the study area (Figure 10). As anthropogenic activities in Seebachtal are largely negligible, this area is a good example of natural processes driving habitat changes. Although the history of human activities in terms of land is important in landscape formation, former and recent natural disturbances (avalanches, rockfall, mudslides) play a major role for the distribution of vegetation types [69]. However, in most cases, spatially referenced data on historic disturbances are difficult to achieve [72].

In our study, based on the obtained intersection matrix, for the largest part of the study area (80% or approximately 4,000 ha), no obvious temporal changes were detected. This was mainly the case for the habitat types forest, rock/rock debris, and snow/glaciers. The other 20% showed some changes, in particular, retrogression from forest to grassland/

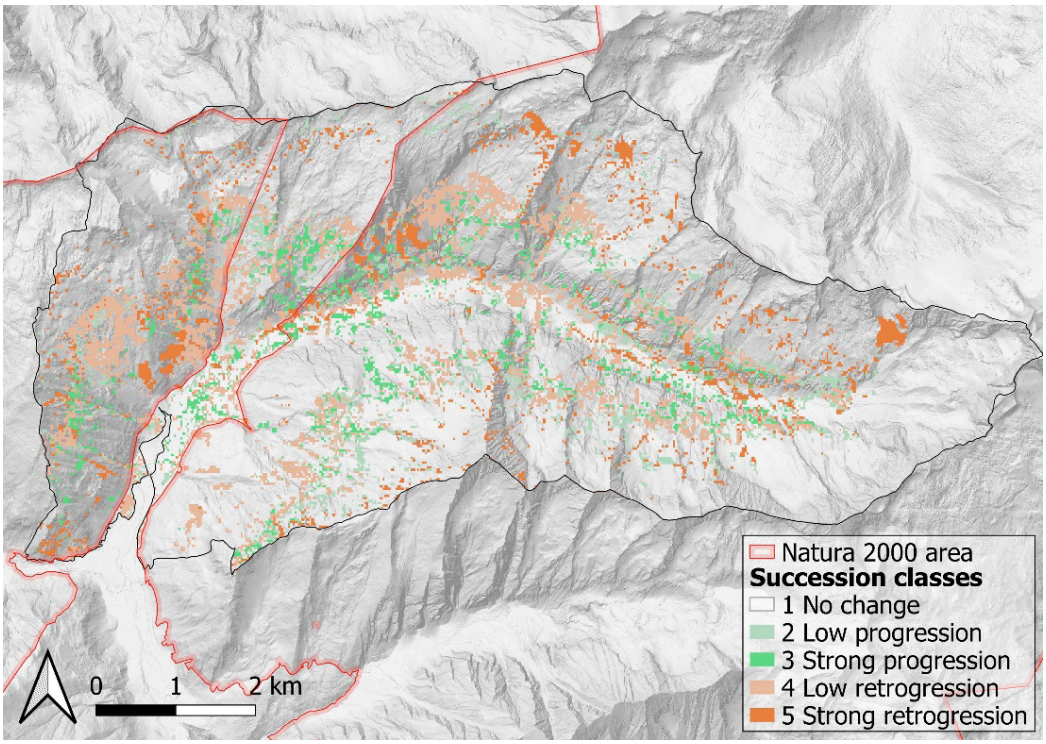

Fig. 10

Figure 10: Map of Seebachtal showing changes in habitat distribution and the resulting successional processes from 1992 to 2022.
Source: own figure

Abbildung 10: *Übersichtskarte über das Seebachtal mit den Veränderungen in der Habitatverteilung und den daraus abgeleiteten Sukzessionsprozessen von 1992 bis 2022. Quelle: eigene Abbildung*

forb/dwarf shrub areas (13%) and succession from grassland/fen areas to forest (7%). Strong retrogression (defined as significant differences between two habitat types) was observed for 5% of the study area, accounting for 236 ha, which is considerable and indicates a high disturbance level, mainly caused by debris flows and landslides. These natural processes can result in the destruction of entire habitats, with high natural dynamics. Low retrogression (defined as insignificant structural differences between two habitat types) was observed for 9% of the study area, accounting for 443 ha. This was characterized by the transformation of forest to grassland/forb/dwarf shrub areas, mainly caused by avalanches. Our results indicate considerable shifts in the dominant habitat types, with natural processes being the dominant driving force. To a low degree, however, the clearance of grey alder forests contributed to retrogression.

Both maps used for the determination of long-term changes were generated using Landsat data, which provide a good classification accuracy. However, when using additional reference points for model calibration, it is important that these points are derived for the same year to enable comparisons. As LiDAR data were not available, some errors were introduced (such as the misclassification of green/grey alder sites), and a direct comparison is therefore only possible to a limited extent.

Conclusions and further outlook

One of the key topics in environmental research is the implementation of standardized and reliable methods for the monitoring of NATURA 2000 sites. To this end, effective, economic, and largely automated methods are required, and the rapidly developing sensor technologies together with advanced image processing methods offer new possibilities in this field [85]. Our novel RS-based approach to classify habitat types in an alpine region yielded promising results, both in terms of habitat classification and delineation. It is particularly suitable for largely undisturbed ecosystems, such as alpine regions. For cultural landscapes, which are subjected to more pronounced human activities, further indices in terms of land use intensity would need to be included. Apart from the considerably high model complexity, water streams and infrastructure are generally difficult to classify. Streams, which usually have a width below 10 m, are below the spatial resolution limit of Sentinel data; this is also the case for roads and tracks, whereas buildings, because of their spectral similarity with rocks and rock debris, cannot yet be classified correctly with our approach.

As a model combining globally available satellite data (Landsat/Sentinel) with site characteristics, Google4Habitat offers a generalized classification method using a well-trained model combined with expert rules and with a hierarchical structure. Ideally, these rules are established in one area and applied in other similar areas, without the need for new reference points. However, to achieve this, a complex artificial intelligence approach is needed to train the model on the different habitat types. Such an approach is highly desirable and requires further research.

REFERENCES

[1] A. Balmford, R. E. Green, and M. Jenkins, "Measuring the changing state of nature," *Trends Ecol. Evol.*, vol. 18, no. 7, pp. 326–330, 2003. doi: 10.1016/S0169-5347(03)00067-3

[2] D. Gonçalves-Souza, P. H. Verburg, and R. Dobrovolski, "Habitat loss, extinction predictability and conservation efforts in the terrestrial ecoregions," *Biol. Conserv.*, vol. 246, p. 108579, Jun. 2020, doi: 10.1016/j.biocon.2020.108579

[3] L. Maiorano, A. Falcucci, E. O. Garton, and L. Boitani, "Contribution of the Natura 2000 network to biodiversity conservation in Italy," *Conserv. Biol.*, vol. 21, no. 6, pp. 1433–1444, 2007, doi: 10.1111/j.1523-1739.2007.00831.x

[4] F. Pedrotti, "Types of vegetation maps", in *Plant and Vegetation Mapping*, 2013, p. 103–181, doi: 10.1007/978-3-642-30235-0_6

[5] C. Corbane, S. Lang, K. Pipkins, S. Alleaume, M. Deshayes, V. E. García Millán, et al., "Remote sensing for mapping natural habitats and their conservation status – New opportunities and challenges," *Int. J. Appl. Earth Obs. Geoinf.*, vol. 37, pp. 7–16, May 2015, doi: 10.1016/j.jag.2014.11.005

[6] C. Tockner, M. S. Lorang, and J. A. Stanford, "River flood plains are model ecosystems to test general hydrogeomorphic and ecological concepts," *River Res. Appl.*, vol. 26, no. 1, pp. 76–86, 2010, doi: 10.1002/rra.1328

[7] S. T. A. Pickett, J. Wu, and M. L. Cadenasso, "Patch dynamics and the ecology of disturbed ground: A framework for synthesis", in *Ecosystems of Disturbed Ground*, Amsterdam, 1999, p. 707–722.

[8] L. Petersen, C. K. Dahl, and K. H. Esbensen, "Representative mass reduction in sampling—A critical survey of techniques and hardware," *Chemom. Intell. Lab. Syst.*, vol. 74, no. 1, pp. 95–114, Nov. 2004, doi: 10.1016/j.chemolab.2004.03.020

[9] P. Li, Q. Wang, T. Endo, X. Zhao, and Y. Kakubari, "Soil organic carbon stock is *Geoderma* closely related to aboveground vegetation properties in cold-temperate mountainous forests,", vol. 154, no. 3–4, pp. 407–415, Jan. 2010, doi: 10.1016/j.geoderma.2009.11.023

[10] H. Zhang, C. Zhan, J. Xia, and P. J. F. Yeh, "Responses of vegetation to changes in terrestrial water storage and temperature in global mountainous regions," *Sci. Total Environ.*, vol. 851, p. 158416, Dec. 2022, doi: 10.1016/j.scitotenv.2022.158416

[11] M. Fontaine, R. Aerts, K. Özkan, A. Mert, S. Gülsoy, H. Süel, et al., "Elevation and exposition rather than soil types determine communities and site suitability in Mediterranean mountain forests of southern Anatolia, Turkey," *For. Ecol. Manage.*, vol. 247, no. 1–3, pp. 18–25, Aug. 2007, doi: 10.1016/j.foreco.2007.04.021

[12] A. C. Edwards, R. Scalenghe, and M. Freppaz, "Changes in the seasonal snow cover of alpine regions and its effect on soil processes: A review," *Quat. Int.*, vol. 162–163, pp. 172–181, Mar. 2007, doi: 10.1016/j.quaint.2006.10.027

[13] Y. Qi, H. Wang, X. Ma, J. Zhang, and R. Yang, "Relationship between vegetation phenology and snow cover changes during 2001–2018 in the Qilian Mountains," *Ecol. Indic.*, vol. 133, p. 108351, Dec. 2021, doi: 10.1016/j.ecolind.2021.108351

[14] R. Benavides, A. Escudero, L. Coll, P. Ferrandis, R. Ogaya, F. Gouriveau, et al., "Recruitment patterns of four tree species along elevation gradients in Mediterranean mountains: Not only climate matters," *For. Ecol. Manage.*, vol. 360, pp. 287–296, Jan. 2016, doi: 10.1016/j.foreco.2015.10.043

[15] L. D. Estes, P. R. Reillo, A. G. Mwangi, G. S. Okin, and H. H. Shugart, "Remote sensing of structural complexity indices for habitat and species distribution modeling," *Remote Sens. Environ.*, vol. 114, no. 4, pp. 792–804, Apr. 2010, doi: 10.1016/j.rse.2009.11.016

[16] J. Vanden Borre, D. Paelinckx, C. A. Mücher, L. Kooistra, B. Haest, G. De Blust, et al., "Integrating remote sensing in Natura 2000 habitat monitoring: Prospects on the way forward," *J. Nat. Conserv.*, vol. 19, no. 2, pp. 116–125, May 2011, doi: 10.1016/j.jnc.2010.07.003

[17] A. Viña, S. Bearer, H. Zhang, Z. Ouyang, and J. Liu, "Evaluating MODIS data for mapping wildlife habitat distribution," *Remote Sens. Environ.*, vol. 112, no. 5, pp. 2160–2169, May 2008, doi: 10.1016/j.rse.2007.09.012

[18] S. Weiers, M. Bock, M. Wissen, and G. Rossner, "Mapping and indicator approaches for the assessment of habitats at different scales using remote sensing and GIS methods," *Landsc. Urban Plan.*, vol. 67, no. 1–4, pp. 43–65, Mar. 2004, doi: 10.1016/S0169-2046(03)00028-8

[19] F. Betz, M. Lauermann, and G. Egger, "Biogeomorphology from space: Analyzing the dynamic interactions between hydromorphology and vegetation along the Naryn River in Kyrgyzstan based on dense satellite time series", *Remote Sens. Environ.*, vol. 299, p. 113890, Dec. 2023, doi: 10.1016/j.rse.2023.113890

[20] F. Betz, M. Lauermann, and B. Cyffka, "Geomorphological characterization of rivers using virtual globes and digital elevation data: A case study from the Naryn River in Kyrgyzstan," *Int. J. Geoinformatics*, vol. 17, no. 1, pp. 47–55, 2021, doi: 10.52939/ijg.v17i1.1707

[21] R. C. Grecchi, R. Beuchle, Y. E. Shimabukuro, L. E. O. C. Aragão, E. Arai, D. Simonetti, et al., "An integrated remote sensing and GIS approach for monitoring areas affected by selective logging: A case study in northern Mato Grosso, Brazilian Amazon," *Int. J. Appl. Earth Obs. Geoinf.*, vol. 61, pp. 70–80, Sep. 2017, doi: 10.1016/j.jag.2017.05.001

[22] I. D. Thompson, M. R. Guariguata, K. Okabe, C. Bahamondez, R. Nasi, V. Heymell, et al., "An operational framework for defining and monitoring forest degradation," *Ecol. Soc.*, vol. 18, no. 2, art. 20, 2013, doi: 10.5751/ES-05443-180220

[23] R. H. Fraser, I. Olthof, and D. Pouliot, "Monitoring land cover change and ecological integrity in Canada's national parks," *Remote Sens. Environ.*, vol. 113, no. 7, pp. 1397–1409, Jul. 2009, doi: 10.1016/j.rse.2008.06.019

[24] J. T. Kerr and M. Ostrovsky, "From space to species: Ecological applications for remote sensing," *Trends Ecol. Evol.*, vol. 18, no. 6, pp. 299–305, 2003, doi: 10.1016/S0169-5347(03)00071-5

[25] J. J. Nossin, "Slope visibility and shadows in side-loop SPOT imagery," ISPRS J. Photogramm. *Remote Sens.*, vol. 46, no. 3, pp. 133–146, Jun. 1991, doi: 10.1016/0924-2716(91)90031-P

[26] I. M. S. Eddy, S. E. Gergel, N. C. Coops, G. M. Henebry, J. Levine, H. Zerriffi, et al., "Integrating remote sensing and local ecological knowledge to monitor rangeland dynamics," *Ecol. Indic.*, vol. 82, pp. 106–116, Nov. 2017, doi: 10.1016/j.ecolind.2017.06.033

[27] Z. Xie, S. R. Phinn, E. T. Game, D. J. Pannell, R. J. Hobbs, P. R. Briggs, et al., "Using Landsat observations (1988–2017) and Google Earth Engine to detect vegetation cover changes in rangelands - A first step towards identifying degraded lands for conservation," *Remote Sens. Environ.*, vol. 232, p. 111317, Oct. 2019, doi: 10.1016/j.rse.2019.111317

[28] J. Dong, X. Xiao, M. A. Menarguez, G. Zhang, Y. Qin, D. Thau, et al., "Mapping paddy rice planting area in northeastern Asia with Landsat 8 images, phenology-based algorithm and Google Earth Engine," *Remote Sens. Environ.*, vol. 185, pp. 142–154, Nov. 2016, doi: 10.1016/j.rse.2016.02.016

[29] A. Retallack, G. Finlayson, B. Ostendorf, K. Clarke, and M. Lewis, "Remote sensing for monitoring rangeland condition: Current status and development of methods," *Environmental and Sustainability Indicators*, vol. 19, p. 100285, Sep. 2023, doi: 10.1016/j.indic.2023.100285

[30] S. Yousefi, M. Avand, P. Yariyan, H. R. Pourghasemi, S. Keesstra, S. Tavangar, et al., "A novel GIS-based ensemble technique for rangeland downward trend mapping as an ecological indicator change," *Ecol. Indic.*, vol. 117, p. 106591, Oct. 2020, doi: 10.1016/j.ecolind.2020.106591

[31] W. Mücke, A. Zlinsky, M. Hollaus, and N. Pfeifer, "Towards operative habitat mapping using airborne laser scanning - the Changehabits2 project", in *ForestSat 2012 Conference*, 2012.

[32] X. Lyu, X. Li, D. Dang, H. Dou, X. Xuan, S. Liu, et al., "A new method for grassland degradation monitoring by vegetation species composition using hyperspectral remote sensing," *Ecol. Indic.*, vol. 114, p. 106310, Jul. 2020, doi: 10.1016/j.ecolind.2020.106310

[33] L. Gao, X. Wang, B. A. Johnson, Q. Tian, Y. Wang, J. Verrelst, et al., "Remote sensing algorithms for estimation of fractional vegetation cover using pure vegetation index values: A review," *ISPRS J. Photogramm. Remote Sens.*, vol. 159, pp. 364–377, Jan. 2020, doi: 10.1016/j.isprsjprs.2019.11.018

[34] Y. Chen, J. P. Guerschman, Z. Cheng, and L. Guo, "Remote sensing for vegetation monitoring in carbon capture storage regions: A review," *Appl. Energy*, vol. 240, pp. 312–326, Apr. 2019, doi: 10.1016/j.apenergy.2019.02.027

[35] V. Lawley, M. Lewis, K. Clarke, and B. Ostendorf, "Site-based and remote sensing methods for monitoring indicators of vegetation condition: An Australian review," *Ecol. Indic.*, vol. 60, pp. 1273–1283, Jan. 2016, doi: 10.1016/j.ecolind.2015.03.021

[36] C. Gómez, J. C. White, and M. A. Wulder, "Optical remotely sensed time series data for land cover classification: A review," *ISPRS J. Photogramm. Remote Sens.*, vol. 116, pp. 55–72, Jun. 2016, doi: 10.1016/j.isprsjprs.2016.03.008

[37] G. le Maire, C. Marsden, Y. Nouvellon, C. Grinand, R. Hakamada, J.-L. Stape, et al., "MODIS NDVI time-series allow the monitoring of Eucalyptus plantation biomass," *Remote Sens. Environ.*, vol. 115, no. 10, pp. 2613–2625, Oct. 2011, doi: 10.1016/j.rse.2011.05.017

[38] Z. Xiao, S. Liang, J. Wang, B. Jiang, and X. Li, "Real-time retrieval of Leaf Area Index from MODIS time series data," *Remote Sens. Environ.*, vol. 115, no. 1, pp. 97–106, Jan. 2011, doi: 10.1016/j.rse.2010.08.009

[39] N. Mueller, A. Lewis, D. Roberts, S. Ring, R. Melrose, J. Sixsmith, et al., "Water observations from space: Mapping surface water from 25 years of Landsat imagery across Australia," *Remote Sens. Environ.*, vol. 174, pp. 341–352, Mar. 2016, doi: 10.1016/j.rse.2015.11.003

[40] D. K. Bolton, J. M. Gray, E. K. Melaas, M. Moon, L. Eklundh, and M. A. Friedl, "Continental-scale land surface phenology from harmonized Landsat 8 and Sentinel-2 imagery," *Remote Sens. Environ.*, vol. 240, p. 111685, Apr. 2020, doi: 10.1016/j.rse.2020.111685

[41] K. Wang, S. E. Franklin, X. Guo, and M. Cattet, "Remote sensing of ecology, biodiversity and conservation: A review from the perspective of remote sensing specialists," *Sensors*, vol. 10, no. 11, pp. 9647–9667, 2010, doi: 10.3390/s101109647

[42] N. Gorelick, M. Hancher, M. Dixon, S. Ilyushchenko, D. Thau, and R. Moore, "Google Earth Engine: Planetary-scale geospatial analysis for everyone," *Remote Sens. Environ.*, vol. 202, pp. 18–27, Dec. 2017, doi: 10.1016/j.rse.2017.06.031

[43] J. Padarian, B. Minasny, and A. B. McBratney, "Using Google's cloud-based platform for digital soil mapping," *Comput. Geosci.*, vol. 83, pp. 80–88, Oct. 2015, doi: 10.1016/j.cageo.2015.06.023

[44] I. Cârlan, B. A. Mihai, C. Nistor, and A. Große-Stoltenberg, "Identifying urban vegetation stress factors based on open access remote sensing imagery and field observations," *Ecol. Inform.*, vol. 55, p. 101032, Jan. 2020, doi: 10.1016/j.ecoinf.2019.101032

[45] X. Zhang, P. M. Treitz, D. Chen, C. Quan, L. Shi, and X. Li, "Mapping mangrove forests using multi-tidal remotely-sensed data and a decision-tree-based procedure," *Int. J. Appl. Earth Obs. Geoinf.*, vol. 62, pp. 201–214, Oct. 2017, doi: 10.1016/j.jag.2017.06.010

[46] A. M. Dewan and Y. Yamaguchi, "Land use and land cover change in Greater Dhaka, Bangladesh: Using remote sensing to promote sustainable urbanization," *Appl. Geogr.*, vol. 29, no. 3, pp. 390–401, Jul. 2009, doi: 10.1016/j.apgeog.2008.12.005

[47] Z. Dezso, J. Bartholy, R. Pongracz, and Z. Barcza, "Analysis of land-use/land-cover change in the Carpathian region based on remote sensing techniques," *Phys. Chem. Earth Parts ABC*, vol. 30, no. 1–3, pp. 109–115, Jan. 2005, doi: 10.1016/j.pce.2004.08.017

[48] J. Jiang and G. Tian, "Analysis of the impact of Land use/Land cover change on Land Surface Temperature with Remote Sensing," *Procedia Environ. Sci.*, vol. 2, pp. 571–575, Jan. 2010, doi: 10.1016/j.proenv.2010.10.062

[49] W. Zhan, Y. Chen, J. Zhou, J. Wang, W. Liu, J. Voogt, et al., "Disaggregation of remotely sensed land surface temperature: Literature survey, taxonomy, issues, and caveats," *Remote Sens. Environ.*, vol. 131, pp. 119–139, Apr. 2013, doi: 10.1016/j.rse.2012.12.014

[50] I. Chawla, L. Karthikeyan, and A. K. Mishra, "A review of remote sensing applications for water security: Quantity, quality, and extremes," *J. Hydrol.*, vol. 585, p. 124826, Jun. 2020, doi: 10.1016/j.jhydrol.2020.124826

[51] C. Giardino, G. Candiani, M. Bresciani, Z. Lee, S. Gagliano, and M. Pepe, "BOMBER: A tool for estimating water quality and bottom properties from remote sensing images," *Comput. Geosci.*, vol. 45, pp. 313–318, Aug. 2012, doi: 10.1016/j.cageo.2011.11.022

[52] K. E. Sawaya, L. G. Olmanson, N. J. Heinert, P. L. Brezonik, and M. E. Bauer, "Extending satellite remote sensing to local scales: Land and water resource monitoring using high-resolution imagery," *Remote Sens. Environ.*, vol. 88, no. 1–2, pp. 144–156, Nov. 2003, doi: 10.1016/j.rse.2003.04.006

[53] C. E. Torgersen, R. N. Faux, B. A. McIntosh, N. J. Poage, and D. J. Norton, "Airborne thermal remote sensing for water temperature assessment in rivers and streams," *Remote Sens. Environ.*, vol. 76, no. 3, pp. 386–398, Jun. 2001, doi: 10.1016/S0034-4257(01)00186-9

[54] S. R. Maniyath and K. Leena, "Rural Built-Up Area Extraction from satellite Images Using Deep Neural Network," *AIP Conf. Proc.*, vol. 2914, no. 1, p. 050011, Dec. 2023, doi: 10.1063/5.0176046

[55] Y. Tan, S. Xiong, and P. Yan, "Multi-branch convolutional neural network for built-up area extraction from remote sensing image," *Neurocomputing*, vol. 396, pp. 358–374, Jul. 2020, doi: 10.1016/j.neucom.2018.09.106

[56] T. T. Werner, A. Bebbington, and G. Gregory, "Assessing impacts of mining: Recent contributions from GIS and remote sensing," *Extr. Ind. Soc.*, vol. 6, no. 3, pp. 993–1012, Jul. 2019, doi: 10.1016/j.exis.2019.06.011

[57] M. A. Wulder, J. G. Masek, W. B. Cohen, T. R. Loveland, and C. E. Woodcock, "Opening the archive: How free data has enabled the science and monitoring promise of Landsat," *Remote Sens. Environ.*, vol. 122, pp. 2–10, Jul. 2012, doi: 10.1016/j.rse.2012.01.010

[58] M. A. Wulder, T. R. Loveland, D. P. Roy, C. J. Crawford, J. G. Masek, C. E. Woodcock, et al., "Current status of Landsat program, science, and applications," *Remote Sens. Environ.*, vol. 225, pp. 127–147, May 2019, doi: 10.1016/j.rse.2019.02.015

[59] F. Vuolo, M. Neuwirth, M. Immitzer, C. Atzberger, and W. T. Ng, "How much does multi-temporal Sentinel-2 data improve crop type classification?" *Int. J. Appl. Earth Obs. Geoinf.*, vol. 72, pp. 122–130, Oct. 2018, doi: 10.1016/j.jag.2018.06.007

[60] R. Chastain, I. Housman, J. Goldstein, M. Finco, and K. Tenneson, "Empirical cross sensor comparison of Sentinel-2A and 2B MSI, Landsat-8 OLI, and Landsat-7 ETM+ top of atmosphere spectral characteristics over the conterminous United States," *Remote Sens. Environ.*, vol. 221, pp. 274–285, Feb. 2019, doi: 10.1016/j.rse.2018.11.012

[61] S. Huang, L. Tang, J. P. Hupy, Y. Wang, and G. Shao, "A commentary review on the use of normalized difference vegetation index (NDVI) in the era of popular remote sensing," *J. For. Res.*, vol. 32, no. 1, pp. 1–6, 2021, doi: 10.1007/s11676-020-01155-1

[62] C. J. Tucker, "Red and photographic infrared linear combinations for monitoring vegetation," *Remote Sens. Environ.*, vol. 8, no. 2, pp. 127–150, May 1979, doi: 10.1016/0034-4257(79)90013-0

[63] J. W. Jr. Rouse, R. H. Haas, Deering. D. W., J. A. Schell, and J. C. Harlan, "Monitoring the vernal advancement and retrogradation (green wave effect) of natural vegetation," Texas A&M University, College Station, TX, USA, Rep. no. NASA-CR-139243 PR-7 E74-10676, Nov. 1974. Accessed: Apr. 5, 2024. [Online]. Available: https://ntrs.nasa.gov/citations/19740022555

[64] G. Egger, "Vegetationsökologische Untersuchungen Seebachtal, Nationalpark Hohe Tauern. Band 1: Vegetation und Standortsdynamik alpiner Lebensräume," Institut für Ökologie und Umweltplanung on behalf of the Federal Ministry for the Environment, Youth and Family Affairs, Klagenfurt, Carinthia, Austria, 1996.

[65] K. Krainer, "Die Geologie der Hohen Tauern," Univ. Publishers, Carinthia, Austria, 1994.

[66] S. Zhang, X. Li, M. Zhong, X. Zhu, and D. Cheng, "Learning k for kNN classification," *ACM Trans. Intell. Syst. Technol.*, vol. 8, no. 3, pp. 1–19, 2017.

[67] L. Breiman, "Random Forests," *Mach. Learn.*, vol. 45, no. 1, pp. 5–32, 2001. doi: 10.1023/A:1010933404324

[68] QGIS Association, "QGIS: A Free and Open Source Geographic Information System". 2024. qgis.org. Accessed: Apr. 5, 2024. [Online]. https://qgis.org/

[69] U. Tappeiner, E. Tasser, and G. Tappeiner, "Modelling vegetation patterns using natural and anthropogenic influence factors: Preliminary experience with a GIS based model applied to an Alpine area," *Ecol. Modell.*, vol. 113, no. 1–3, pp. 225–237, Nov. 1998, doi: 10.1016/S0304-3800(98)00145-8

[70] H. S. Fischer, "Simulating the distribution of landscape communities in an alpine landscape," *Coenoses*, vol. 5, no. 1, pp. 37–43, 1990.

[71] G. del Barrio, B. Alvera, J. Puigdefabregas, and C. Diez, "Respnse of high mountain landscape to topographic variables: Central pyrenees," *Landsc. Ecol.*, vol. 12, no. 2, pp. 95–115, 1997. doi: 10.1007/BF02698210

[72] B. Hoersch, G. Braun, and U. Schmidt, "Relation between landform and vegetation in alpine regions of Wallis, Switzerland. A multiscale remote sensing and GIS approach," *Comput. Environ. Urban Syst.*, vol. 26, no. 2–3, pp. 113–139, Mar. 2002, doi: 10.1016/S0198-9715(01)00039-4

[73] S. Jacek, "Landform characterization with geographic information systems," *Photogramm. Eng. Remote Sensing*, vol. 63, no. 2, pp. 183–191, 1997.

[74] H. Kirchmeir, C. Keusch, and S. Lieb, "Biotopkataster – Kartierrichtlinie. Naturrauminformationssystem Kärnten – NIS-K," E.C.O. Institute for Ecology. Published by the Office of the Carinthian Provincial Government, Department 8, 2018.

[75] T. Ellmauer, V. Igel, H. Kudrnovsky, D. Moser, and D. Paternoster, "Monitoring von Lebensraumtypen und Arten von gemeinschaftlicher Bedeutung in Österreich 2016-2018 und Grundlagenerstellung für den Bericht gemäß Art.17 der FFH-Richtlinie im Jahr 2019: Teil: Kartieranleitungen," On behalf of the Austrian federal states. Umweltbundesamt GmbH, Vienna, 2019.

[76] T. Ellmauer, "Entwicklung von Kriterien, Indikatoren und Schwellenwerten zur Beurteilung des Erhaltungszustandes der Natura 2000-Schutzgüter. Band 3: Lebensraumtypen des Anhangs I der Fauna- Flora-Habitat-Richtlinie," Commissioned by the nine Austrian provinces, the Federal Ministry of Agriculture, Forestry, Environment and Water Management and the Federal Environment Agency, 2005.

[77] H. Yu, W. Ni, Z. Zhang, G. Sun, and Z. Zhang, "Regional forest mapping over mountainous areas in Northeast China using newly identified critical temporal features of Sentinel-1 backscattering," *Remote Sens.*, vol. 12, no. 9, p. 1485, 2020, doi: 10.3390/rs12091485

[78] A. Dostálová, M. Hollaus, M. Milenković, and W. Wagner, "Forest area derivation from Sentinel-1 data," *ISPS Annals of the Photogrammetry, Remote Sensing and Spatial Information Sciences*, 2016.

[79] J. N. Hansen, E. T. A. Mitchard, and S. King, "Assessing forest/non-forest separability using Sentinel-1 C-band synthetic aperture radar," *Remote Sens.*, vol. 12, no. 11, p. 1899, 2020, doi: 10.3390/rs12111899

[80] D. Kopeć, D. Michalska-Hejduk, Ł. Sławik, T. Berezowski, M. Borowski, et al., "Application of multisensoral remote sensing data in the mapping of alkaline fens Natura 2000 habitat," *Ecol. Indic.*, vol. 70, pp. 196–208, Nov. 2016, doi: 10.1016/j.ecolind.2016.06.001

[81] M. C. Alonso and J. A. Malpica, "Satellite imagery classification with LIDAR data," *International Archives of the Photogrammetry, Remote Sensing and Spatial Information Science*, 2010.

[82] A. Novelli, M. A. Aguilar, A. Nemmaoui, F. J. Aguilar, and E. Tarantino, "Performance evaluation of object based greenhouse detection from Sentinel-2 MSI and Landsat 8 OLI data: A case study from Almería (Spain)," *Int. J. Appl. Earth Obs. Geoinf.*, vol. 52, pp. 403–411, Oct. 2016, doi: 10.1016/j.jag.2016.07.011

[83] D. Phiri, M. Simwanda, S. Salekin, V. R. Nyirenda, Y. Murayama, and M. Ranagalage, "Sentinel-2 data for land cover/use mapping: A review," *Remote Sens.*, vol. 12, no. 14, p. 2291, 2020, doi: 10.3390/rs12142291

[84] A. Chakhar, D. Ortega-Terol, D. Hernandez-Lopez, R. Ballesteros, J. F. Ortega, and M. A. Moreno, "Assessing the accuracy of multiple classification algorithms for crop classification using Landsat-8 and Sentinel-2 data," *Remote Sens.*, vol. 12, no. 11, p. 1835, 2020, doi: 10.3390/rs12111735

[85] M. Förster, A. Frick, H. Walentowski, and B. Kleinschmit, "Approaches to utilising QuickBird data for the monitoring of NATURA 2000 habitats," *Community Ecol.*, vol. 9, no. 2, pp. 155–168, 2008, doi: 10.1556/ComEc.9.2008.2.4

ABOUT THE AUTHORS

Gregory Egger
Karlsruher Institut für Technologie (KIT), Institut für Geographie und Geoökologie (IfGG), Abteilung Aueninstitut, Rastatt, Germany
Naturraumplanung Egger, Klagenfurt am Wörthersee, Austria
Universität für Bodenkultur Wien, Institut für Hydrobiologie und Gewässermanagement Vienna, Austria
E-Mail: gregory.egger@naturraumplanung.at

Stephan Preinstorfer
Naturraumplanung Egger, Klagenfurt am Wörthersee, Austria

Marlene Kollmann
Naturraumplanung Egger, Klagenfurt am Wörthersee, Austria

Isabell Becker
Karlsruher Institut für Technologie (KIT), Institut für Geographie und Geoökologie (IfGG), Abteilung Aueninstitut, Rastatt, Germany

Emma Izquierdo-Verdiguier
Universität für Bodenkultur Wien, Institut für Geomatik, Vienna, Austria

Miriam Paul
Naturraumplanung Egger, Klagenfurt am Wörthersee, Austria

BACK TO CONTENT